2011

Lattice distortions and oxygen vacancies produced in Au+-irradiated nanocrystalline cubic zirconia

Philip D. Edmondson
Oak Ridge National Laboratory

William J. Weber
Oak Ridge National Laboratory, weberwj@ornl.gov

Fereydoon Namavar
University of Nebraska Medical Center

Yanwen Zhang
Oak Ridge National Laboratory, zhangy1@ornl.gov

Lattice distortions and oxygen vacancies produced in Au+-irradiated nanocrystalline cubic zirconia

Philip D. Edmondson,[a] William J. Weber,[a,b] Fereydoon Namavar[c] and Yanwen Zhang[a,b,*]

[a]Materials Science and Technology Division, Oak Ridge National Laboratory, Oak Ridge, TN 37831, USA
[b]Department of Materials Science & Engineering, University of Tennessee, Knoxville, TN 37996, USA
[c]University of Nebraska Medical Center, Omaha, NE 68198, USA

The oxygen ion conductivity, attributed to an oxygen vacancy mechanism, of yttria-stabilized zirconia membranes used in solid oxide fuel cells is restricted due to trapping limitations. In this work, a high concentration of oxygen vacancies has been deliberately introduced into nanocrystalline stabilizer-free zirconia through ion-irradiation. Oxygen vacancies with different charge states can be produced by varying irradiation temperatures. Due to the reduced trapping sites and high oxygen vacancy concentration, this work suggests that the efficiency of solid oxide fuel cells can be improved.
Published by Elsevier Ltd. on behalf of Acta Materialia Inc.

Keywords: Nanocrystalline zirconia; Oxygen vacancy; Lattice spacing; Glancing incidence X-ray diffraction; Ion-beam modification

Yttria-stabilized zirconia is used as an oxygen-ion-conducting solid electrolyte in many devices, such as sensors and solid oxide fuel cells, due to its extraordinary oxygen transport properties, which are attributed to an oxygen vacancy mechanism [1]. The stabilization of zirconia with an aliovalent compound such as yttria (Y_2O_3) serves a dual purpose in the system. First, pure zirconia exists in three different thermodynamically stable polymorphs at atmospheric pressure: a monoclinic phase at temperatures below 1400 °C, a tetragonal phase at temperatures of 1400–2600 °C and a cubic phase at temperatures above 2600 °C. The cubic phase is the most interesting phase as an engineering material due to its isotropic expansion at various temperatures. By doping the zirconia with an aliovalent compound with concentrations of ∼8–10 mol.% [1–5], the cubic phase of zirconia is stabilized at the temperatures typically experienced during the operation of oxygen sensors and fuel cells through the introduction of structural oxygen vacancies into the lattice. Secondly, the oxygen vacancies that serve to stabilize the zirconia also lead to the fast oxygen ion conductivity desired in many

applications [2,3]. However, studies have shown that increase of the dopant concentration greater than ∼10 mol.% reduces the ion conductivity [6,7]. This reduction in ion conductivity has been suggested to occur as a result of numerous mechanisms: phase transformation to the tetragonal phase of ZrO_2, precipitation of ordered phases such as $Y_2Zr_2O_7$, formation of microdomains, segregation of yttria to grain boundaries, and short-range ordering arising from the trapping of oxygen vacancies by the dopant cations [8]. Therefore the ion conductivity in stabilized zirconia films is maximized when doping with concentrations of ∼8–10 mol.%. It is therefore of technological interest to improve the oxygen ion conductivity in zirconia by introducing a high concentration of oxygen vacancies without the introduction of stabilizing elements.

Nanostructured materials, i.e. those having grain sizes well below 100 nm, are leading a technological revolution. This is in part due to their exceptional size-dependent chemical, physical, optical and electrical properties compared to those of their micron-sized polycrystalline and single crystal counterparts [9–13]. Nanostructured materials are therefore attracting significant interest for use in a wide variety of applications, such as catalysts, advanced nuclear energy systems, solar cells, membranes, oxygen sensors and solid oxide fuel cells.

Recently, it has been demonstrated that it is possible to produce nanocrystalline tetragonal or cubic zirconia

* Corresponding author at: Materials Science and Technology Division, Oak Ridge National Laboratory, Oak Ridge, TN 37831, USA. Tel.: +1 865 574 8518; fax: +1 865 241 3650; e-mail: zhangy1@ornl.gov

that is thermodynamically stable at atmospheric pressures without the addition of stabilizers [10,13,14], i.e. they are nanostructurally stabilized. Furthermore, the grain size of pure cubic nanostructurally stabilized zirconia (NSZ) films can be tailored by varying the ion dose during energetic, heavy ion irradiation [14]. Moreover, a significant loss of oxygen is also reported, suggesting the production of oxygen vacancies as a result of the irradiation [14]. Thus it may be possible to tailor the oxygen vacancy content, and hence the oxygen ion conductivity, in cubic NSZ by ion irradiation that could lead to much higher ionic conductivity than that obtained in dopant-stabilized zirconia films, where the conductivity is often limited by the interactions between the oxygen vacancies and the stabilizing elements, as described previously. This would serve to improve the reliability and heat management of solid oxide fuel cells, e.g. by enabling a lower operating temperature.

To date, most research has focused on radiation processes (primarily heavy ion irradiation) in either partially- or fully stabilized zirconia as single crystals or with micron-sized grains, or on nanograined ZrO_2 that are either embedded in a foreign matrix or as free-standing particles [15–17]. The work presented here examines the effect of heavy ion irradiation on NSZ with a view to understanding the defect production, saturation and evolution of oxygen vacancies, and how this impacts the unit cell structure.

Thin films, approximately 300 nm thick, of NSZ in the cubic phase with initial grain sizes of 5–10 nm have been grown on top of a (0 0 1) Si substrate using an ion-beam-assisted deposition technique [10]. These films have previously been shown to be structurally stable up to temperatures of 1123 K [5,10]. The films were then irradiated with 2 MeV Au^+ ions at a temperature of 160 or 400 K over a range of doses up to ~35 displacements per atom (dpa). The energy was chosen such that the energy deposited into the film was maximized whilst minimizing the number of ions implanted into the film. Subsequent to the irradiation, samples were analyzed using the complimentary techniques of glancing incidence X-ray diffraction (GIXRD) and cross-sectional transmission electron microscopy (XTEM). The GIXRD was performed using Cu $K_{\alpha1}$ X-rays. Specimens to be examined using XTEM
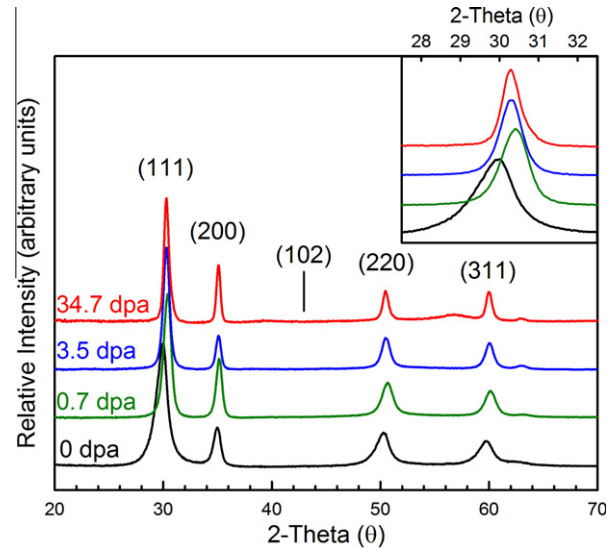

Figure 1. GIXRD spectra obtained for the as-deposited film and the films irradiated by 2 MeV Au at 400 K. The irradiation doses and the diffraction indices, including the absent (1 0 2) index, are labelled. The inset shows a magnified view of the (1 1 1) peak.

were prepared by tripod polishing followed by ion milling to perforation using a Gatan PIPS. A JEOL 2010 transmission electron microscope operating at 200 keV was used to image the specimens.

The curves shown in Figure 1 are the GIXRD results for the 400 K samples for the as-deposited (0 dpa) sample, and those irradiated to doses of 0.7, 3.5 and 35 dpa. It can be seen that the as-deposited sample is the cubic polymorph. This is inferred by the absence of the (1 0 2) reflection at ~43°, which is characteristic of the tetragonal phase. As the dose is increased up to 35 dpa, there is no peak observed at ~43°, indicating that the cubic phase is retained despite the significant energy deposition to the lattice during the irradiation. The absence of the tetragonal phase is confirmed by the selected area electron diffraction (SAED) patterns obtained during XTEM, as shown in Figure 2a and b for the as-deposited sample and the sample irradiated to ~35 dpa at 400 K, respectively. The SAED patterns also indicate that there is a grain-coarsening effect occurring.
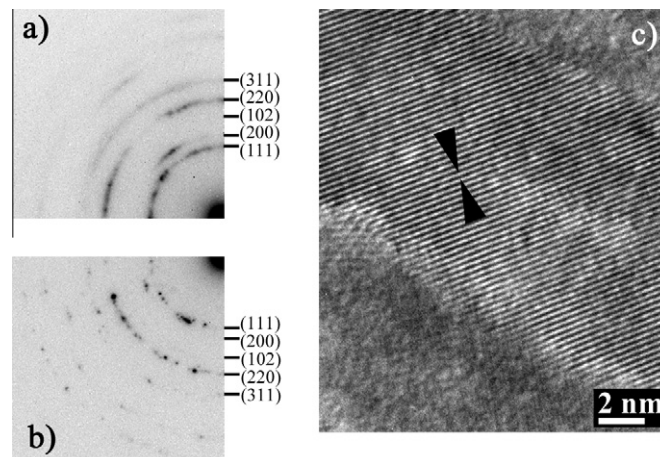

Figure 2. SAED patterns of (a) the as-deposited film and (b) the film irradiated by 2 MeV Au to a dose of ~35 dpa at 400 K. (c) A high-resolution TEM image of a typical grain in the as-deposited film. The arrows indicate a d_{111} spacing of 2.51 Å.

This is concluded from the transition of the diffuse SAED pattern in Figure 2a to a much sharper pattern with discrete diffraction spots becoming visible in Figure 2b. This grain-coarsening observation was attributed to a defect-stimulated grain growth mechanism [14]. The SAED patterns further indicate that the nanocrystalline grains are arranged in random orientations.

The inset shown in Figure 1 is a magnified view of the (1 1 1) peaks obtained by GIXRD. Two observations are immediately apparent: the narrowing of the peaks with increasing irradiation dose (dpa) and the shift in the positioning of the peaks. The narrowing of the peaks corresponds to the grain coarsening discussed earlier [14]. However, the shift in the peaks is related to a change in the spacing of the (1 1 1) planes, d_{111}. This, in turn, is related to a change in the lattice parameter a (proportional to d_{111} by a factor of $\sqrt{3}$). The high-resolution micrograph shown in Figure 2c is of (1 1 1) lattice fringes from a typical grain in the as-deposited NSZ film. The lattice spacing indicated by the arrows is 2.51 Å, as calculated using a fast Fourier transform of the grain in the image. This is in close agreement with measurements obtained from the GIXRD (2.369 Å), but is significantly lower than the theoretical value for cubic zirconia of 2.962 Å [18]. GIXRD is a more accurate method for measuring lattice spacing than high-resolution TEM and allows more grains to be sampled.

Figure 3a shows the percentage difference between the d_{111} spacings measured by GIXRD and the theoretical d_{111} spacing as a function of dpa. Measurements of the higher order reflections gave the same results, but the (1 1 1) reflections are used here to allow for comparison with the TEM measurements. This result shows that, for the as-deposited film, there is a significant compression of the lattice from the ideal, represented by contraction of approximately -20% from the theoretical d_{111}. This demonstrates that the lattice is highly stressed despite the use of Ar ions during the deposition process to relieve the stress [10]. The 400 K irradiation (open triangles and the dashed line) shows that there is a significant increase in the d_{111} spacing compared to that of the as-deposited material of greater than $\sim27\%$ at low dpa. This indicates that there is a substantial amount of radiation induced stress relief in the system. Immediately following this stress relief phase, the d_{111} spacing begins to reduce, before approaching a stable stress value of $\sim-2\%$. A similar effect is observed for the 160 K irradiation (open squares, solid line), although the initial relaxation phase is not quite so dramatic as for the 400 K irradiation. Here the d_{111} spacing, under 160 K irradiation, tends to stabilize at $\sim-9\%$. The result in Figure 3b shows the change in overall thickness of the film, measured by XTEM, as a function of dose. It is evident that the film thickness follows a similar trend to that of the d_{111} spacing measurements. These correlated events indeed indicate that ion irradiation is an efficient tool to modify and control the lattice parameter throughout the film.

Previous studies have shown that a may reduce significantly as a function of grain size for powdered nanocrystalline CeO_2, particularly in the size range of the grains of interest here (3–30 nm) [19]. However, in the previous study, the effects of the unconstrained free surface may not be negligible. Moreover, the results shown
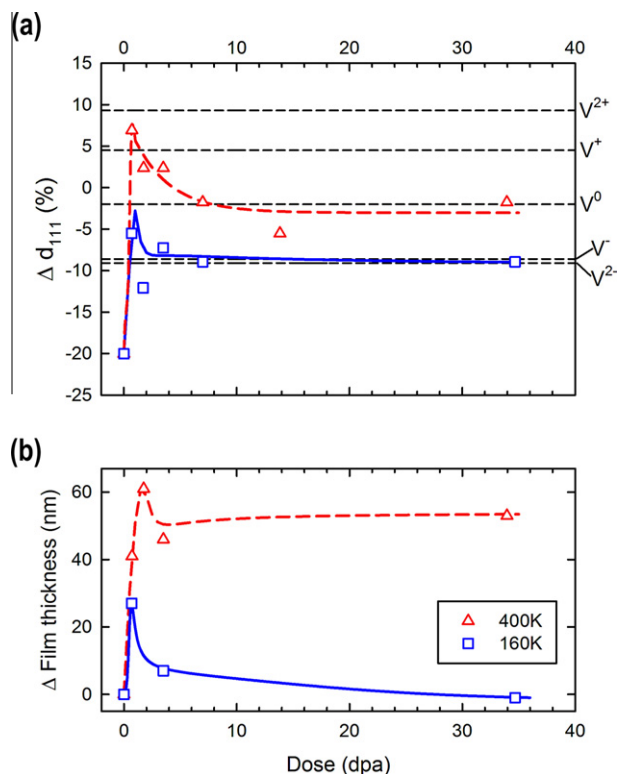

Figure 3. (a) A plot of the difference between the ideal d_{111} spacing and that measured by GIXRD (as a percentage) as a function of dose. The distortions induced by oxygen vacancies with different charge states are overlaid. (b) A plot of the variation in film thickness measured by XTEM as a function of dose. The lines serve to guide the eye.

in Figure 4a, particularly for the 160 K irradiation, show that, whilst there is a relatively large increase in grain size of ~6 nm (from 23.5 to 29.5 nm) from 8 to 35 dpa, there is little, if any, change in d_{111}. This demonstrates that the variation in lattice parameter observed here is a result not of the change in the grain size, but of a different mechanism altogether. To understand the mechanism by which the lattice parameter changes, the types of defect, their accumulation and saturation in the NSZ films are evaluated. Whilst different configurations of defects may be formed in zirconia, such as the oxygen interstitials and anti-site defects, by far the most common defect is the oxygen vacancy. The oxygen di-vacancy has been observed [20], but only during swift heavy-ion irradiations performed at 8 K. The graph shown in Figure 4b shows that there is a significant loss of O (up to $\sim19\%$) as a result of the irradiation, and hence the most likely defect to exist in significant quantities is the isolated oxygen vacancies. An ab initio study of isolated oxygen vacancies in nanocrystalline cubic zirconia [18] has shown that five different charge states of the defect may exist: V^{2+}, V^+, V^0, V^- and V^{2-}. In the same study, it was shown that the production of an oxygen vacancy could result in a change in the atom–atom distances in the neighborhood of the defect, the amount of distortion being dependent on the charge state of the defect. The distortions are: 9.3% (V^{2+}), 4.5% (V^+), -2.0% (V^0), -8.6% (V^-) and -9.1% (V^{2-}), with positive values representing a lattice expansion, negative values a lattice contraction. The positively and neutrally charged defects are symmetrical, whilst the negatively charged
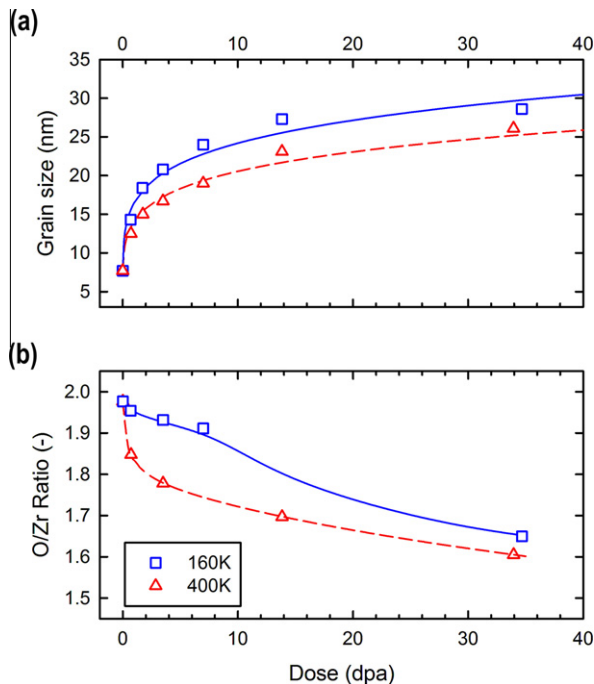
Figure 4. Plots of the grain size (a) and the O/Zr ratio (b) as a function of dose for both the 160 and 400 K irradiations. The lines in all the plots are to serve as a guide to the eye.

vacancies are asymmetrical and hence the distortion stated above is for the maximum asymmetric displacement of the atom–atom distance.

In Figure 3a the distortions produced by the oxygen vacancies of the different charge states are overlaid. It can be seen that, as the vacancy defects begin to saturate within the nanocrystalline matrix or along the grain boundaries at an ion dose exceeding 10 dpa, three types of defects are the most likely to exist: V^0, V^{2-} and V^-. For the 400 K irradiation, the V^0 defect appears to be the dominant defect. For the 160 K irradiation, it is not quite so clear, with both the V^{2-} and V^- defects producing similar distortions to the lattice; however, it suggests that these two defects may be the dominant defects at 160 K. Electron paramagnetic resonance experiments [17] performed on γ-ray-irradiated monoclinic ZrO_2 has shown that the V^- defect is the most likely to exist, leading to the possibility that this is the most dominant defect at 160 K. This cannot be categorically proven, however, as the difference in the crystal structures (monoclinic phase versus cubic phase) may lead to different charge states being dominant.

It is clear that there is a thermal component to the stability of the V^0, V^{2-} and V^- defects. As the negative charge state vacancies are not dominant at the higher 400 K irradiation, this is an indication that, at some temperature between 160 and 400 K, these defects may become mobile, leading to interaction and annihilation of the defects or neutralization to the V^0 defect. The V^0 defect is clearly thermodynamically stable at 400 K.

In, conclusion it has been shown that there is a significant alteration to the lattice parameter resulting from heavy ion irradiation. The change in the lattice parameter, inferred by a change in the d_{111} spacing, is due to the production and saturation of oxygen vacancies of differ-

ent charge states, and the extent of the lattice distortion is dependent on the charge state of the oxygen vacancies produced. We have shown that, at 400 K, the neutral charge state oxygen vacancy, V^0, is the dominant defect, while at 160 K the V^{2-} and V^- charge states may be the dominant defects. These results also show that the negatively charged oxygen vacancies are not thermodynamically stable at elevated temperatures, i.e. those above 400 K.

[1] U. Brossmann, R. Wurschum, U. Sodervall, H.-E. Schaefer, J. Appl. Phys. 85 (1999) 7646–7654.
[2] B.W. Busch, W.H. Schulte, E. Garfunkel, T. Gustafsson, W. Qi, R. Nieh, J. Lee, Phys. Rev. B 62 (2000) R13290.
[3] G. Knöner, K. Reimann, R. Röwer, U. Södervall, H.-E. Schaefer, Proc. Natl. Acad. Sci. USA 100 (2003) 3870–3873.
[4] R. Devanathan, W.J. Weber, S.C. Singhal, J.D. Gale, Solid State Ionics 177 (2006) 1251–1258.
[5] Y.L. Soo, P.J. Chen, S.H. Huang, T.J. Shiu, T.Y. Tsai, Y.H. Chow, Y.C. Lin, S.C. Weng, S.L. Chang, G. Wang, C.L. Cheung, R.F. Sabirianov, W.N. Mei, F. Namavar, H. Haider, K.L. Garvin, J.F. Lee, H.Y. Lee, P.P. Chu, J. Appl. Phys. 104 (2008) 113535-1–113535-5.
[6] A.I. Ioffe, D.S. Rutman, S.V. Karpachov, Electrochim. Acta 23 (1978) 141–142.
[7] S.P.S. Badwal, Solid State Ionics 52 (1992) 23–32.
[8] J. Kondoh, S. Kikuchi, Y. Tomii, Y. Ito, J. Electrochem. Soc. 145 (1998) 1536–1550.
[9] A.P. Alivisatos, Science 271 (1996) 933–937.
[10] F. Namavar, C.L. Cheung, R.F. Sabirianov, W.-N. Mei, X.C. Zeng, G. Wang, H. Haider, K.L. Garvin, Nano Lett. 8 (2008) 988–996.
[11] D.J. Norris, A.L. Efros, S.C. Erwin, Science 319 (2008) 1776–1779.
[12] M.V. Kovalenko, M. Scheele, D.V. Talapin, Science 324 (2009) 1417–1420.
[13] J. Lian, J. Zhang, F. Namavar, Y. Zhang, F. Lu, H. Haider, K. Garvin, W.J. Weber, R.C. Ewing, Nanotechnology 20 (2009) 245303.
[14] Y. Zhang, W. Jiang, C. Wang, F. Namavar, P.D. Edmondson, Z. Zhu, F. Gao, J. Lian, W.J. Weber, Phys. Rev. B 82 (2010) 184105.
[15] A. Benyagoub, Phys. Rev. B 72 (2005) 094114.
[16] D.G. Lamas, A.M. Rosso, M.S. Anzorena, A. Fernández, M.G. Bellino, M.D. Cabezas, N.E. Walsöe de Reca, A.F. Craievich, Scripta Mater. 55 (2006) 553–556.
[17] S. Wright, R.C. Barklie, J. Appl. Phys. 106 (2009) 103915–103917.
[18] D. Muñoz Ramo, P.V. Sushko, J.L. Gavartin, A.L. Shluger, Phys. Rev. B 78 (2008) 235432.
[19] S. Deshpande, S. Patil, S.V.N.T. Kuchibhatla, S. Seal, Appl. Phys. Lett. 87 (2005) 133113-1–133113-3.
[20] J.-M. Costantini, F. Beuneu, K. Schwartz, C. Trautmann, J. Phys.: Condens. Matter 22 (2010) 315402.